A Numerical Study of Beam-to-Column Joints Subjected to Impact

E. L. Grimsmo[*], A. H. Clausen, A. Aalberg, M. Langseth

Structural Impact Laboratory (SIMLab) and Centre for Advanced Structural Analysis (CASA), Department of Structural Engineering, Norwegian University of Science and Technology, NO-7491 Trondheim, Norway
[*]Corresponding author. Email address: erik.l.grimsmo@ntnu.no.

Abstract

Limited documentation is concerned with the behaviour of steel joints subjected to severe impulsive loading originating from incidents such as explosions or impact. In this paper, finite element simulations are used to investigate the behaviour of beam-to-column joints with bolted end-plate connections subjected to impact loading. An elastic-thermoviscoplastic material model was employed in the simulations. Good agreement was obtained between the simulations and previously reported tests in terms of both global and local behaviour. In particular, the numerical model successfully reproduced the experienced failure mode of tensile bolt fracture combined with end-plate deformation. The validated model was employed in investigations of three cases, in which the main findings are as follows: 1) reducing the end-plate thickness significantly increased the energy dissipated by the joint; 2) axial forces in the beams only marginally affected the response; and 3) including the additional inertia introduced by the presence of floor slabs may change the failure mode to premature shear failure.

Keywords: beam-to-column joints; finite element simulations; end-plate connections; steel; impact loading; dynamic behaviour

1 Introduction

In the past 15-20 years, particularly after the attack on the World Trade Center in 2001, there has been increased interest in the behaviour of joints subjected to extreme dynamic loads. The beam-to-column joints in a framed structure should preferably be able to transmit such loads to the

surrounding members without failing. This requires that the joints have adequate properties such as energy dissipation capacity, which can be considered as a combined measure of the strength and ability to deform before failure. Similarly, design code UFC 3-340-02: *Structures to resist the effects of accidental explosions* [1] states that the main frame connections must be designed for strength, stiffness, and rotational capacity in the case of blast loading. Nevertheless, current design codes provide few guidelines on the design of beam-to-column joints for extreme impulsive loading conditions. In addition, there is only limited research on the topic.

Dynamic tests on full-scale joints can increase our knowledge of this topic, but such experiments are expensive and challenging to perform in a controlled manner. Compared to quasi-static tests, a well-defined application of the load is more difficult to achieve in the dynamic case, and more advanced instrumentation tools are required. The interaction between the joint and its surrounding structure is also challenging to consider in experiments; therefore, it is common to only perform tests on the joint itself and on a minor part of the adjacent beam and column members. An example of such an interaction is when large deformations of a framed structure induce considerable axial forces in the beams through catenary action. In addition, the interaction with structural components such as floor slabs is impractical to include in experiments. Considering floor slabs is particularly important under severe dynamic load conditions. This is because these members introduce considerable inertia, which may significantly alter the response compared to the quasi-static case. Moreover, it is difficult to accurately investigate parameters such as energy dissipation in the different components of the joints based on experimental data. Such challenges related to the testing of joints can be readily addressed with numerical simulations. A trustworthy numerical investigation requires that the model is validated. This means that the model is able to capture the experienced global as well as local response of the joint at hand, including the correct failure mode.

Few reports on numerical analyses of the transient dynamic response of beam-to-column joints can be found in the literature. Sabuwala et al. [2] studied the behaviour of beam-to-column joints subjected to blast loads. A pressure load was imposed on a finite element (FE) model of single-sided, beam-to-column joints with bolted fin-plate connections. The load represented the pressure originating from an internal explosion within a hypothetical room. It was observed that the recommendations from a design code (the precursor to UFC 3-340-02 [1]) were inadequate. A

limitation of the study is that the FE model was only validated against physical experiments conducted under quasi-static load conditions.

For some years, researchers at the Nanyang Technological University have performed experiments and FE simulations to investigate the behaviour of various steel connections during a so-called column-loss scenario; see, for instance, Yang and Tan [3]. Most relevant to the current study are the papers by Liu et al. [4-6] because they applied the load in a dynamic manner. They observed good agreement between the global displacement-time curves obtained from the experiments and simulations.

A comprehensive experimental programme commenced a few years ago at the University of Sheffield, where a purpose-built test rig has been used to study the behaviour of single-sided joints subjected to high loading rates; see Tyas et al. [7]. Rahbari et al. [8] simulated both quasi-static and dynamic tests on web-cleat connections performed with this test rig. They observed that their model captured the main aspects of the response, including the failure mode. A parametric study by Rahbari et al. revealed that the thickness of the web-cleat angles had only a minor effect on the moment resistance of the connection but that it strongly affected its rotational capacity.

Grimsmo et al. [9] tested double-sided, beam-to-column joint configurations both quasi-statically and dynamically. The test specimens consisted of two H-section beams connected with an H-section column using extended end-plates and high-strength bolts. The dynamic tests were conducted with a test rig designed for impact testing of structural components. Failure occurred by tensile bolt fracture combined with end-plate bending deformation in both the quasi-static and dynamic tests. However, it seemed that the ductility and energy dissipation of the test specimen increased with greater impact velocities.

The first objective of this paper is to present and validate a three-dimensional FE model of the impact tests reported by Grimsmo et al. [9]. Compared to most models presented in the relevant literature, the current study incorporates a material model where the strain-rate sensitivity and fracture parameters are calibrated using material test specimens machined from the members used in the beam-to-column joint assembly. The second objective is to demonstrate how a validated model can be employed to investigate aspects that are challenging to explore in physical impact tests. The following investigations were chosen for this paper:

1) How the energy dissipated in the joint region is influenced by minor changes in the design of the joint. This study is limited to varying the end-plate thickness.

2) How axial forces in the beams affect the behaviour of the joint configuration.

3) How the response of the joint configuration is influenced by the inertia of floor slabs attached to the beams. The purpose of this investigation is to provide a qualitative assessment of the inertia effects.

Section 2 of this paper briefly summarizes the laboratory tests in terms of both full-scale component and material tests. Next, Section 3 presents the material model and discusses how the material parameters were identified. The FE model of the impact tests is introduced in Section 4 and subsequently validated in Section 5. The investigations of energy dissipation, axial force, and inertia are presented in Sections 6, 7, and 8, respectively. Finally, concluding remarks are given in Section 9.

2   Laboratory tests

2.1   Test specimen and impact tests

The experimental programme, including impact tests in a pendulum accelerator, was thoroughly presented by Grimsmo et al. [9]. Only a brief survey of the experiments is provided here. A schematic illustration of the test specimen and experimental setup is shown in Figure 1. The specimens consisted of: two HEA 180 sections that served as beams; an HEB 220 section representing the column; an "impact plate" spot welded to the end of the column; two 10 mm web stiffeners welded to the column; two 12 mm extended end-plates that were welded to the beams by fillet welds with throat thicknesses of 5 mm; and a total of twelve partially threaded M16 × 65 bolts of grade 8.8. The H-sections and end-plates were manufactured from grade S355 steel. Additional dimensions relevant to the modelling are provided in the Appendix. The test specimen was designed so that several components of the joint experienced plastic deformation, and so that failure occurred by tensile bolt fracture combined with end-plate bending deformation. Thus, a numerical model of the tests may be considered reliable if it can capture this relatively complex deformation mode.
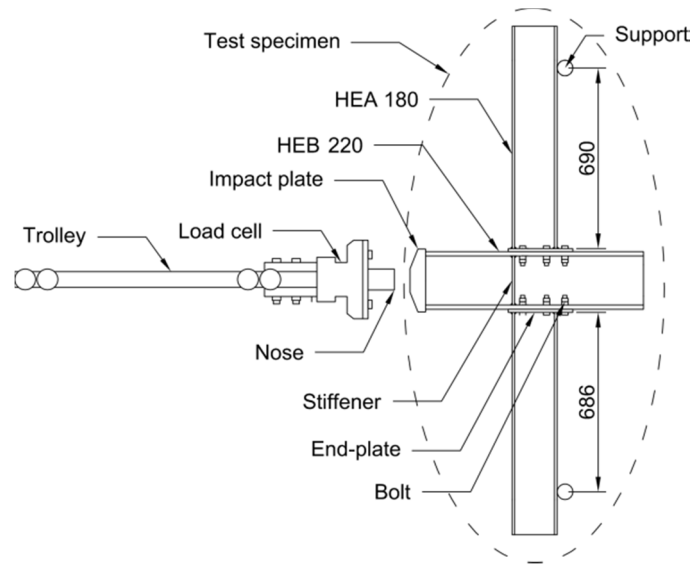
Figure 1 - Elevation view of the impact test setup.

A key part of the pendulum accelerator is the trolley (727 kg) illustrated in Figure 1, which rolled along two rails and impacted the test specimen with a given velocity. Four tests were performed on the specimen geometry in Figure 1: two with an impact velocity of approximately 8 m/s and two with an impact velocity of nearly 12 m/s. The duration of a test, i.e., from impact to bolt failure, was between 5 and 10 milliseconds, depending on the impact velocity of the trolley.

The beams were supported on steel cylinders placed 690 and 686 mm from each end-plate, as observed in Figure 1. Thus, the joints were mainly loaded by bending moments and shear forces as the column displaced horizontally due to the impact. All tests included a high-speed camera that monitored the deformation and fracture process of the region around the upper end-plate in Figure 1. Also, the slight difference in distance to the supports increased the likelihood of failure initiating at the part that was captured by the camera.

2.2   Material tests

Mechanical properties of the different components were determined by performing quasi-static and dynamic uniaxial tension tests. The specimens used in these tests are displayed in Figure 2. Full-thickness specimens (Figure 2a) were taken from the flanges of the sections and the end-plate, and specimens with reduced shank (Figure 2b) were machined from the bolts. Quasi-static tests were

a) Full thickness specimen (for end-plate and H-sections)

b) Bolt specimen
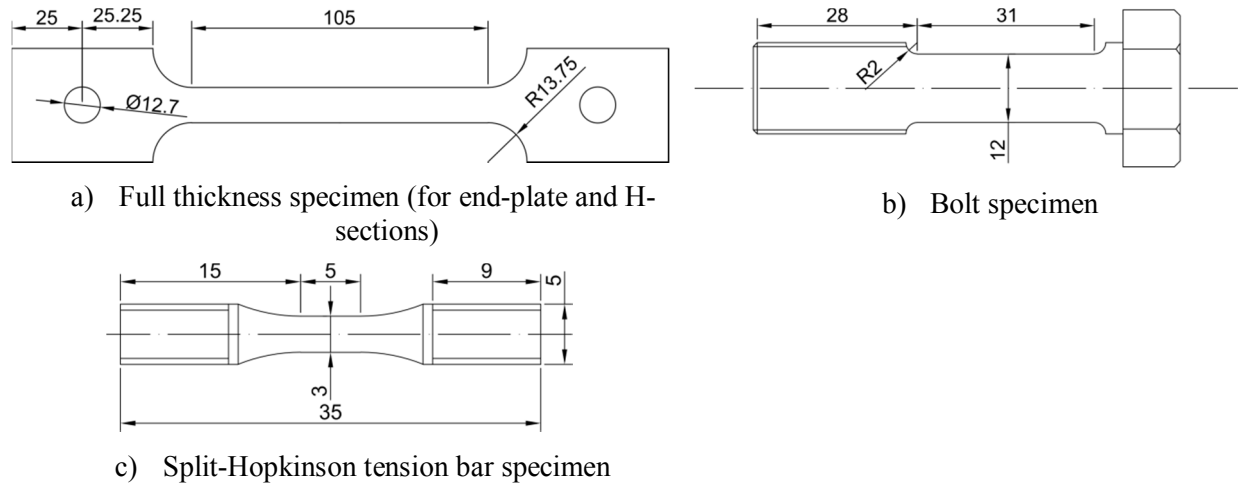
c) Split-Hopkinson tension bar specimen

Figure 2 - Test specimens employed in uniaxial tension tests (measures in mm).

conducted on the specimens in Figure 2a and b in a standard hydraulic machine with a strain rate of the order of 10^{-4} s^{-1}. Digital cameras captured the deformations of the specimens. The specimens were painted with a speckle pattern, which enabled digital image correlation (DIC) analyses. Thus, local strains in the neck and the true stress-strain response up to failure could be determined. Replicate tests were performed, and a good agreement was achieved between the replicates. Some results from these tests are given in Section 3.2. Additional results are provided by Grimsmo et al. [9].

Figure 2c depicts the specimens employed in a strain-rate sensitivity investigation. This specimen was machined from the end-plates and bolts. The materials of the beam and column sections were assumed to have the same strain-rate sensitivity as the end-plate material because all these parts were made of S355 steel. Material tests at strain rates of approximately 10^{-3} and 10^{-1} s^{-1} were obtained with a standard hydraulic machine, and a split-Hopkinson tension bar was employed for testing at strain rates of the order of 10^{2} s^{-1}. The split-Hopkinson tests were conducted with the instrumentation as described by Vilamosa et al. [10]. In Section 3.2, the results from these tests are provided together with the calibrated strain-rate sensitivity parameters.

3   Material model

3.1   Constitutive model and fracture criterion

The materials were modelled with an elastic-thermoviscoplastic constitutive relation that incorporated the following: linear elasticity, the von Mises yield criterion, the associated flow rule, non-linear isotropic hardening, strain-rate hardening, and thermal softening due to adiabatic heating. The equivalent stress σ_{eq} was defined by

$$\sigma_{eq} = \begin{cases} \sigma_y, & \varepsilon_p \leq \varepsilon_{p,plat} \\ \left[\sigma_y + \sum_{i=1}^{2} Q_i \left(1 - \exp\left(-\frac{\theta_i}{Q_i}(\varepsilon_p - \varepsilon_{p,plat})\right)\right)\right]\left[1 + \frac{\dot{\varepsilon}_p}{\dot{\varepsilon}_{ref}}\right]^C [1 - T_h^m], & \varepsilon_p > \varepsilon_{p,plat} \end{cases} \tag{1}$$

where σ_y is the yield stress; Q_i and θ_i, $i = \{1,2\}$, are the hardening constants of the extended Voce hardening rule; ε_p is the equivalent plastic strain; $\varepsilon_{p,plat}$ is the value of ε_p at the end of the yield plateau; $\dot{\varepsilon}_{ref}$ is a reference strain rate that, together with the constant C, governs the rate sensitivity; T_h is the homologous temperature; and m is a constant. The homologous temperature is defined as $T_h = (T - T_r)/(T_m - T_r)$, where T is the absolute temperature, T_r is the room temperature, and T_m is the melting temperature. Because the duration of the simulations is less than 10 milliseconds, heat conduction effects can be neglected. Adiabatic heating is therefore assumed, and the temperature increment is calculated as

$$\Delta T = \int_0^{\varepsilon_p} \chi \frac{\sigma_{eq}}{\rho C_p} d\varepsilon_p$$

where χ is the Taylor-Quinney coefficient, ρ is the density, and C_p is the specific heat capacity.

Failure was included in the simulations by employing the fracture criterion proposed by Cockcroft and Latham [11]. The criterion states that failure occurs when the integral

$$W = \int_0^{\varepsilon_p} \max(\sigma_I, 0) d\varepsilon_p \tag{2}$$

attains a critical value W_{cr}. Here, σ_I is the maximum principal stress. This failure criterion is strain-rate sensitive via the principal stress, cfr. Equation (1). Furthermore, the criterion is indirectly

dependent on stress triaxiality and the Lode angle, as shown by Gruben et al. [12]. In the simulations, the elements were eroded when W reached its critical value W_{cr} at the integration points.

The material model, including the constitutive relations and the failure criterion, were implemented in the simulations by a user subroutine developed and validated at SIMLab.

3.2   Material parameter identification

Table 1 provides the material parameters deduced from the material tests discussed in Section 2.2. These parameters were employed in the simulations of the full-scale joint tests. All four materials (column, beam, plate, and bolt material) were assigned a Young's modulus of 210 GPa, Poisson's ratio of 0.3, and density of 7900 kg/m³.

From the quasi-static tension tests performed on the specimens in Figure 2a and b, true stress-plastic strain curves were obtained, and the yield stress σ_y and the strain $\varepsilon_{p,plat}$ were read directly from representative curves. Initial values of the hardening parameters Q_i and θ_i were acquired by fitting the term in the first square brackets in Equation (1) to the pre-necking values of the true stress-plastic strain curves. For the plate and bolt material, the hardening parameters were subsequently optimised via inverse modelling of the quasi-static tension tests such that the correct response was also obtained for post-necking strains, giving the result in Figure 3. Here, the engineering stress is plotted versus the area reduction at the neck. The inverse modelling procedure was not performed for the column and beam material because only pre-necking plastic strains occurred for these two materials in the full-scale joint tests and simulations.

Table 1 - Material parameters used in the simulations of the full-scale joint tests.

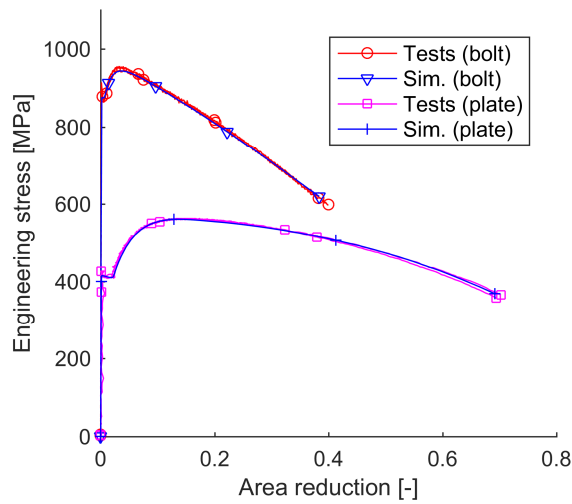|	σ_y [MPa]	Q_1 [MPa]	θ_i [MPa]	Q_2 [MPa]	θ_2 [MPa]	$\varepsilon_{p,plat}$ [-]	$\dot{\varepsilon}_{ref}$ [1/s]	C [-]	W_{cr} [MPa]
Column	404.1	71.8	3442	200.5	2022	0.008	0.001	0.016	-
Beam	438.8	14.2	2804	193.3	3436	0.012	0.001	0.016	-
Plate	413.7	178.5	4610	630.9	508.4	0.020	0.001	0.016	786.0
Bolt	874.0	127.9	4595	13650	303.0	0.008	0.001	0.011	1311

Figure 3 - Curves showing engineering stress versus area reduction of the minimum cross-section obtained from two replicate tension tests performed for the plate and bolt material, and corresponding simulations of the tests.

The parameters $\dot{\varepsilon}_{ref}$ and C were determined by least-square fitting of linear polynomials to the experimental data obtained from the strain-rate sensitivity investigation. Recall that these experimental data were found from tests performed on the end-plate and bolt material used in the full-scale component tests. The results are displayed in Figure 4. Here, the axes are defined such that the slope of the linear curves corresponds to the value of C when the temperature factor in Equation (1) is set to unity. The reference strain rate $\dot{\varepsilon}_{ref}$ was chosen as 10^{-3} s^{-1}, i.e., approximately the lowest strain rate in the investigation involving the test specimen shown in Figure 2c. As observed in Figure 4, the stresses obtained experimentally were acquired at two pre-necking values of the true strain, i.e., 0.09 and 0.16 for the plate material, and 0.04 and 0.07 for the bolt material. The values of C were calculated as the average of the two slopes determined for each of the two materials.
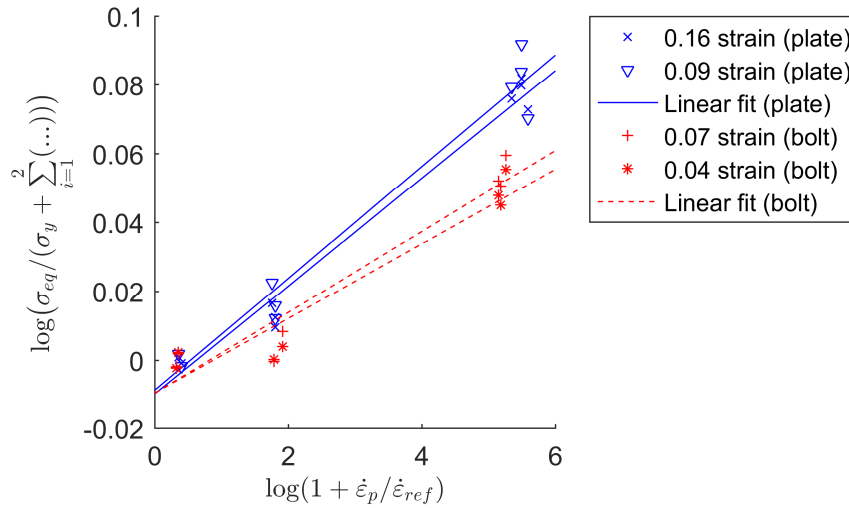
Figure 4 - Flow stress at pre-defined levels of plastic strain as a function of equivalent plastic strain rate for the plate and bolt material.

All four materials were given the following temperature-related parameters: $m = 1.0$, $T_r = 293$ K, $T_m = 1800$ K, $\chi = 0.9$, and $C_p = 452$ J/kgK. These values were adopted from Børvik et al. [13], and are typical for steels.

The fracture parameter W_{cr} was determined by simulating the quasi-static tension tests using elements of the same size as those used in the full-scale joint simulations because W_{cr} is known to be strongly mesh dependent. The simulations were therefore run with element sizes of 3.0 mm and 1.0 mm for the plate and bolt material, respectively. The onset of fracture in the tensile test simulations was defined as the instant when the work, i.e., force integrated over displacement, performed on the specimen equalled the work up to fracture determined by the experiments. At this instant, the largest value of the integral W (see Equation (2)) in the mesh corresponded to the critical value W_{cr}. The fracture parameter was not determined for the column and beam material because these did not exhibit fracture during the tests.

4   Finite element model

The impact tests on the column and beam assembly were simulated using the commercial FE software Abaqus/Explicit [14] with solid elements. A comprehensive script that generated a parameterised model of the tests was written so that minor changes in dimensions and geometry could be readily applied.

4.1   Geometry and discretisation

The FE model of the impact tests is shown in Figure 5. By exploiting symmetry, one half of the physical specimen was modelled; see Figure 5a. Two analytical rigid surfaces with cylindrical shape represented the beam supports. The trolley was modelled as a rigid body with a mass equal to that of the physical trolley, except for the nose of the trolley, which was explicitly modelled and located 0.1 mm from the impact plate at the start of the simulation.

Figure 5b provides a detailed view of the end-plate region. The welds were modelled as triangular parts. Figure 5c shows that the threads of the bolts were not explicitly included in the model because that would require very small elements, which would further lead to impractically small stable time increments in the explicit analyses. The partially threaded bolts were therefore modelled with a smooth shank along the entire length between the head and nut. A representative diameter of 13.9 mm was applied in the threaded portion; see Figure A.3 in the Appendix for additional details about the bolt and nut part. This diameter was deduced from quasi-static tension tests performed on M16 bolt and nut assemblies such that the bolt model would reproduce the maximum force registered during these tests. Note that two nuts per bolt were used in the tests to prevent possible thread failure, and the modelled nut was therefore higher than a single regular nut.

Figure 5b and c show the mesh density of the model. Mesh seeds of 3 mm were applied to the end-plates, which gave 4 elements over the thickness. The column and beams were given mesh seeds of 4 mm. Since significant deformation was experienced by the bolt shank, mesh seeds of approximately 1 mm were applied to this region, which gave 14 elements over the smallest diameter. The remainder of the bolt and nut part was given mesh seeds of approximately 3 mm. Inevitably, somewhat inhomogeneous meshes were obtained due to the challenges related to meshing circular and hexagonal geometries; see Figure 5c. The entire model contained approximately 310 000 elements. The mesh density was considered sufficient because the model produced results that agreed with those obtained from the tests, and because refining the mesh only minimally affected the response. Solid elements with reduced integration (C3D8R) were employed for the entire model, except for the welds, where wedge elements (C3D6) were used.
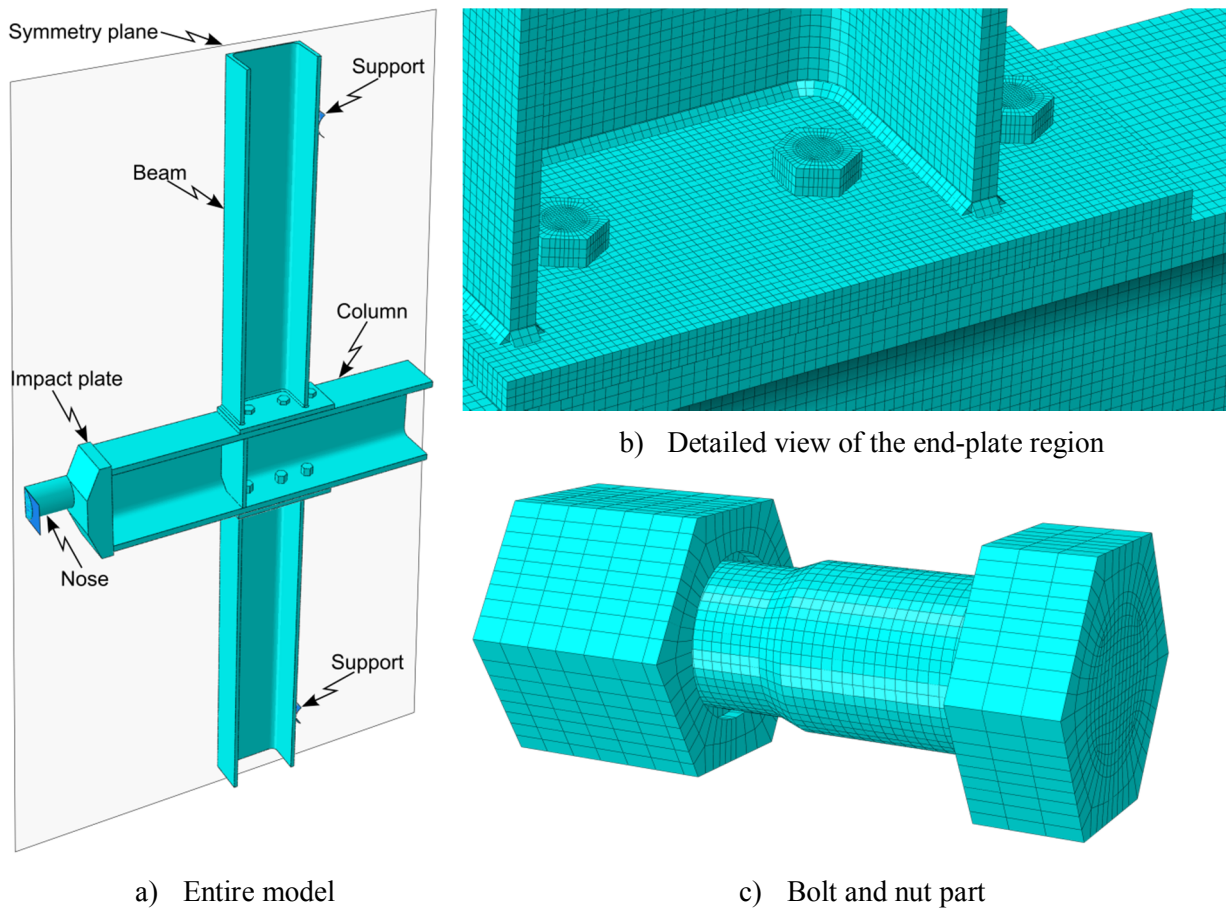
a) Entire model

b) Detailed view of the end-plate region

c) Bolt and nut part

Figure 5 - FE model of the impact tests.

4.2   Boundary and initial conditions

Appropriate boundary conditions ensured that the supports of the beams were fixed in all directions, and that the trolley was only allowed to translate along the column axis. The pre-impact velocity of the trolley measured in the experiments was set as an initial velocity for the trolley in the model.

A tightening moment of 80 Nm was applied to the bolt and nut assemblies in the tests [9]. A pre-study investigated whether a corresponding pre-tensioning of the bolts in the simulations affected the results. No significant effect was observed; therefore, pre-tensioning was not included in the following simulations.

4.3   Constraints and contact

Tie constraints were used to connect the welds to the beams, the welds to the end-plates, the beams to the end-plates, the stiffener to the column, the impact plate to the column, and the nose to the

trolley. Furthermore, a surface-to-surface type of contact was employed using the penalty method contact algorithm. A total of 30 surface pairs for contact were included in the model: bolt heads and end-plates, bolt shanks and bolt holes of end-plates, bolt shanks and bolt holes of column flanges, nuts and column flanges, end-plates and column flanges, supports and beams, column end and impact plate, and nose and impact plate. "Hard contact" was used as the contact property in the normal direction of the contact surfaces, whereas the isotropic Coulomb friction model with a penalty formulation was applied in the tangential direction. The code NS-EN 1090-2: *Execution of steel structures and aluminium structures - Part 2* [15] suggests a friction coefficient of 0.2 for rolled and untreated surfaces. This value was adopted for all contact pairs in the model.

4.4   Materials

In Section 3.2, the material parameters for the column, beams, end-plates, and bolts were presented. The welds were assigned the same material parameters as the beams, whereas the stiffener was given the parameters of the column. Recall that failure is not considered for the beam and column material, and possible failure of the welds is thus not treated in the current study. The impact plate and the nose of the trolley were both machined from high-strength steel, and were assigned the same properties as the bolt material.

5   Validation

The numerical model of the impact tests was validated by demonstrating that the deformation and failure mode experienced in the corresponding tests and simulations were similar. In addition, the response was compared in terms of global force-displacement and velocity-time curves. It is demonstrated in Section 5.1 that the model indeed captures both the local response in the part of the joint that fails and the global response the entire joint. Further, a model of a corresponding quasi-static test is evaluated in Section 5.2.

5.1   Impact test simulation

Figure 6a shows a close-up of the deformed joint observed in a test and simulation 7 milliseconds after the specimen was impacted by the trolley at 12 m/s. The deformation of the end-plate is clearly similar in the test and simulation, and failure occurred by tensile fracture of the centre bolt (row) in both cases. Note that the head of the centre bolt in Figure 6a is not in contact with the end-plate

a) End-plate region approx. 1 ms after fracture in centre bolt

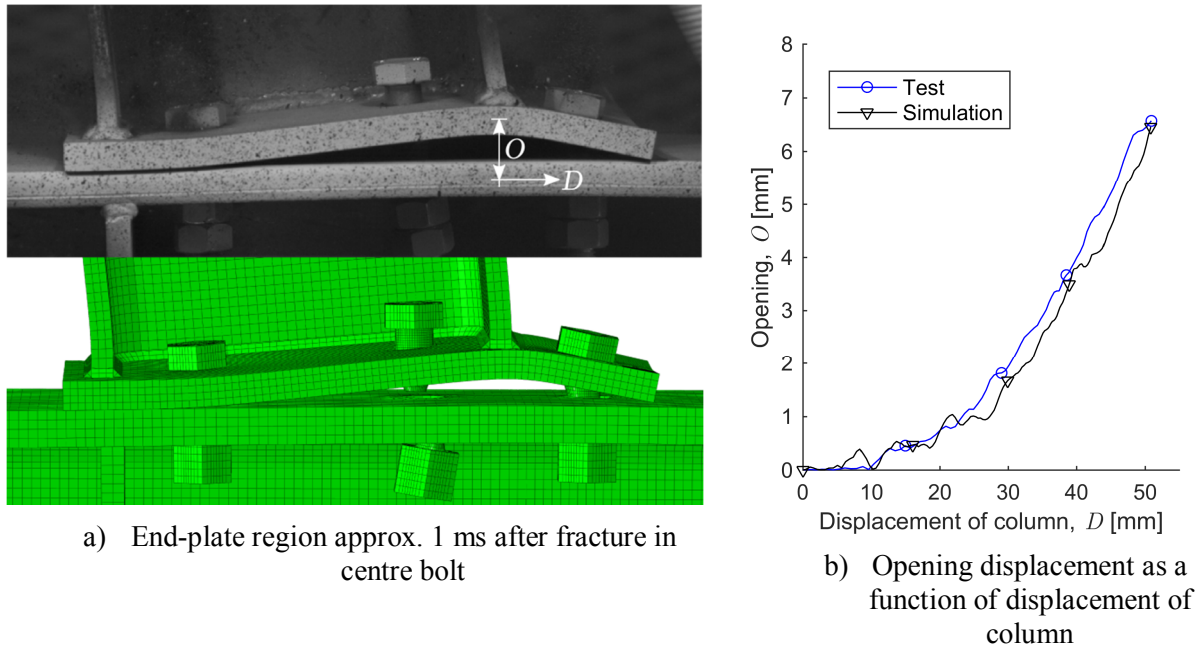b) Opening displacement as a function of displacement of column

Figure 6 - Deformation of end-plate region in an impact test at 12 m/s and corresponding simulation.

in neither the test nor the simulation because fracture had occurred approximately 1 ms earlier. The figure also defines D as the displacement of the column relative to the fixed camera position, and O as the opening displacement between the column flange and end-plate. In Figure 6b, the opening O is plotted versus the displacement D obtained from both DIC analysis and simulation, and a good agreement is observed. The curves in this figure, and all subsequent curves in this paper, are plotted to the instant where bolt fracture was observed in the respective test or simulation. Thus, considering Figure 6b, the applied fracture parameter W_{cr} produced failure at approximately the same displacement D and opening O in the simulation as observed in the test.

Grimsmo et al. [9] estimated that the average strain rate in the threaded length of the fracturing bolt was 130 s^{-1} by measuring the opening between the end-plate and the column flange under the bolt throughout the test. In comparison, the average plastic strain rate was 110 s^{-1} in the elements of the corresponding portion of the bolt in the model. Both the experimentally and numerically obtained strain rates were determined during the period beginning at the start of the tensile deformation of the bolts and ending approximately at the onset of necking. An increase in the strain rate from 0.001 to 110 s^{-1} corresponds to a dynamic enhancement of the equivalent stress by a factor 1.14 according to the bolt material model presented in Section 3.2. Furthermore, at the incipient necking of the bolts in the simulations, the maximum temperature had increased by approximately 45 K,

which reduced the equivalent stress by a factor of only 0.97. However, this factor was 0.84 immediately prior to failure because the maximum temperature had increased by approximately 240 K. This thermal softening resulted in failure at a displacement D equal to 50.9 mm rather than 52.3 mm, which was obtained in a simulation that did not include thermal softening. The response, in terms of force-displacement and deformation mode, was practically unaffected by temperature effects otherwise.

Figure 7 depicts various curves obtained from the two replicate tests with an impact velocity of 12 m/s and the corresponding simulation. The force P acquired from the tests was measured by the load cell shown in Figure 1. In the simulation, the force was defined as the contact force between the nose of the trolley and the impact plate. This difference in force measurement, together with the fact that all contact surfaces were perfectly coplanar in the simulation (most likely not the case in the experiments), explains why the force increased more suddenly in the simulation; see Figure 7a. Moreover, the trolley system was not completely rigid in reality, which may have introduced additional softness to the response in the tests. Nevertheless, the force curve acquired from the simulation agrees reasonably well with the test results. As thoroughly discussed by Grimsmo et al. [9], the two distinct force peaks were caused by two nearly elastic collisions occurring between the trolley and the test specimen during the tests. This is reflected in the velocity V of the column, which is plotted versus time in Figure 7b. The first impact caused an acceleration of the column, and because the area under the force-displacement curve is larger for the simulation, the column obtained greater velocity than in the tests. Thereafter, the column decelerated during the non-contact period (approximately from 1 to 4 ms) because the joints started to resist the translation of the column. During this period, the simulation and tests yielded the same behaviour in terms of velocity, which indicates that the joints have the same resistance in the model and test. The trolley had a constant velocity in the non-contact period and eventually impacted the specimen again at approximately 4 ms. Thus, the column was accelerated a second time, which was also well captured by the simulation. Figure 7c displays the velocity V_t of the trolley as a function of time; good agreement is again observed between the simulation and the test. This implies that the correct amount of kinetic energy was transferred from the trolley to the specimen during impact in the simulation.

a)   Force versus displacement of column

b)   Velocity of column versus time
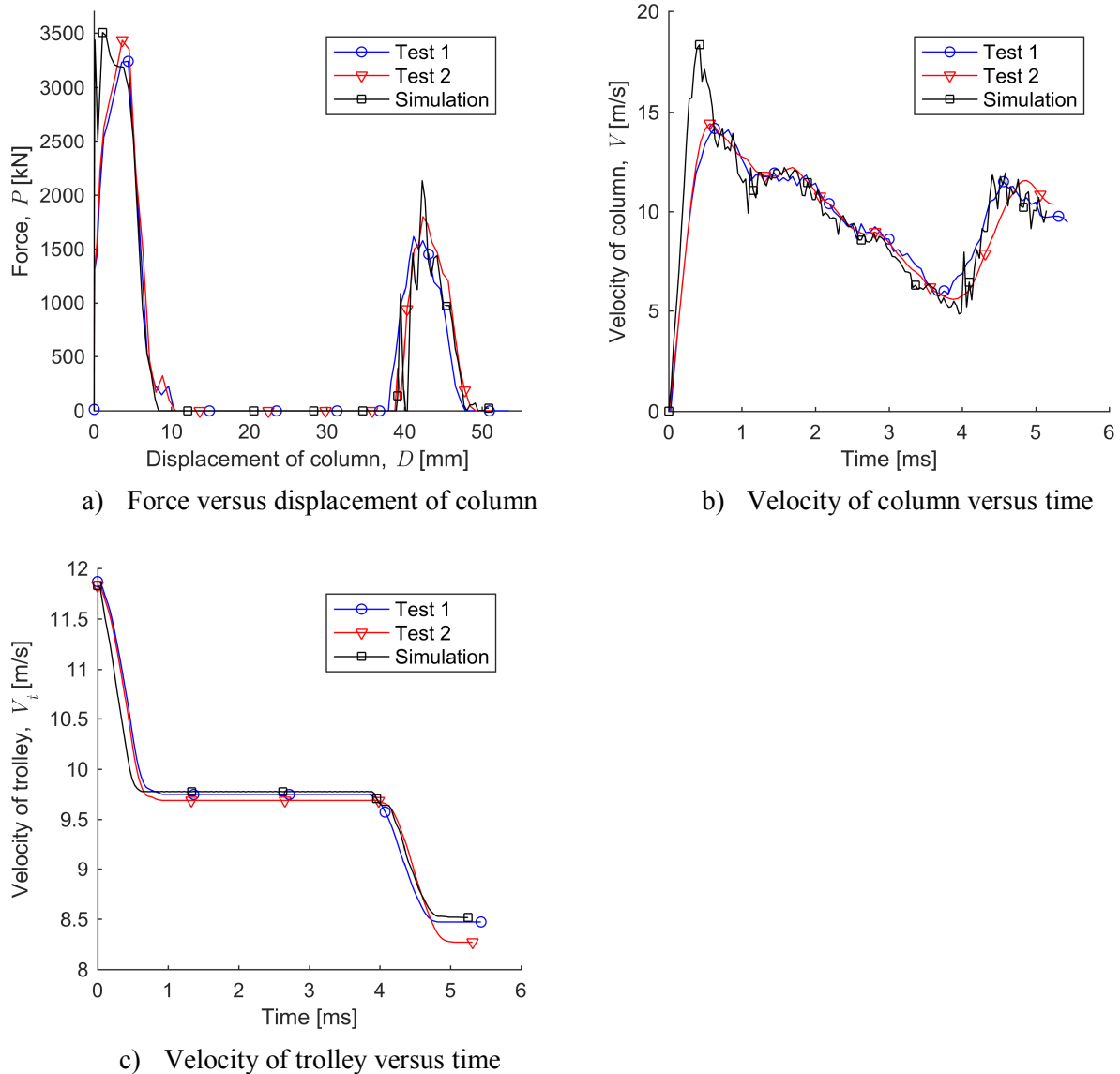

c)   Velocity of trolley versus time

Figure 7 - Response obtained from two replicate impact tests at 12 m/s and corresponding simulation.

5.2   Quasi-static test simulation

For the purpose of complete validation, the quasi-static tests of the beam-to-column joints were also simulated. These tests are described by Grimsmo et al. [9]. An implicit solver in Abaqus/Standard [14] was used to allow for longer integration times so that the effects of inertia forces could be avoided. The main features of the discretisation and material modelling were the same as for the impact test model except that temperature effects were neglected. Without going into further detail about the quasi-static model, Figure 8 and Figure 9 compare the results with the experiments. Note that only one of the two replicate quasi-static tests was monitored with cameras.

Figure 8 shows that the deformation mode is generally similar in the tests and simulation. As experienced in the tests, the deformation became asymmetric with respect to the centreline of the column after obtaining the maximum force in the simulation. This asymmetrical behaviour can be seen from the difference in deformation of the two end-plates in Figure 8. Furthermore, tensile fracture of the bolts occurred at one of the connections in both tests and simulation. However, the magnitude of the asymmetrical behaviour was not the same in the simulation as in the test, and the simulated opening O at failure was smaller than the observed opening in the test; see the curves in Figure 9a.

Figure 9b shows that the force was generally larger in the simulation than in the two tests. On the other hand, satisfactory agreement is found when considering the maximum force.
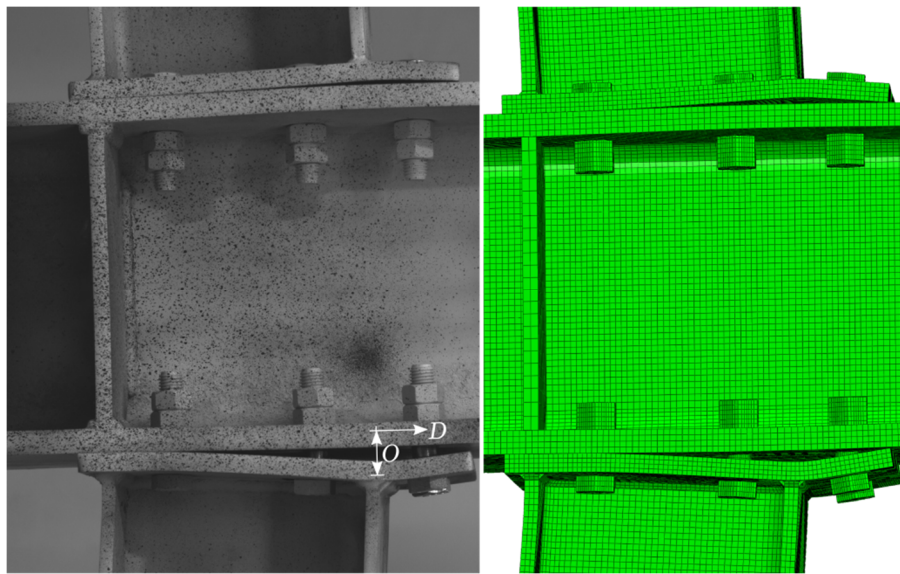

Figure 8 - Deformation of joint region immediately prior to fracture in the quasi-static test and simulation.

a)   Opening versus displacement of column

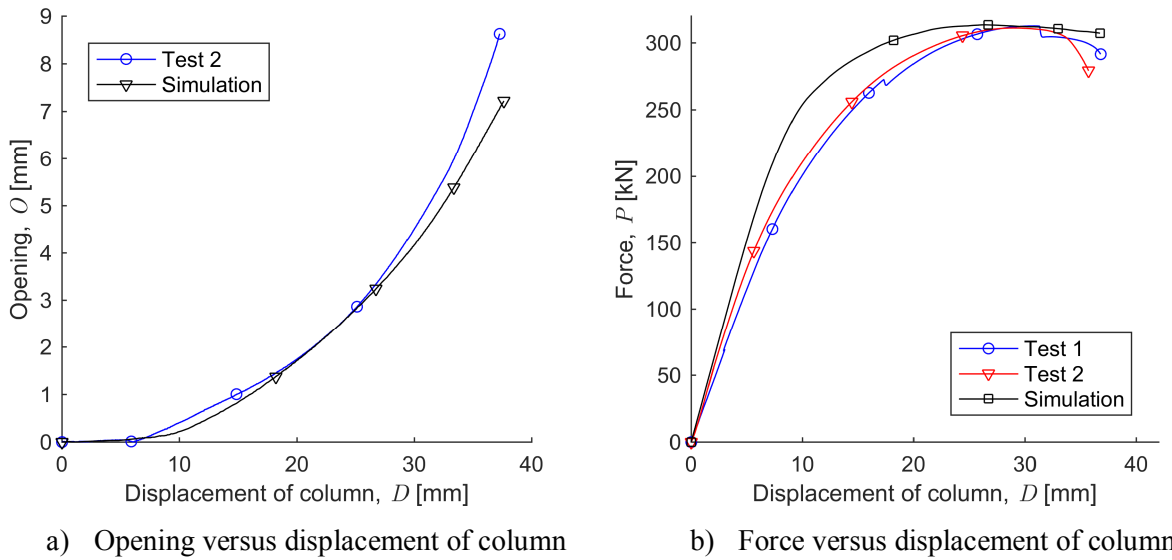b)   Force versus displacement of column

Figure 9 - Curves obtained from two quasi-static tests, whereof one was instrumented with camera, and corresponding simulation.

6   Energy dissipation

The ability to absorb energy is an important property of a structure subjected to dynamic loading. Provided that the validation domain is not exceeded, the numerical model presented in Section 4 can be employed to evaluate how various choices with respect to the joint design affect the energy absorption. FE simulations may also serve to explore differences between quasi-static and dynamic responses. Since the intention of this paper is to demonstrate the methodology, the present study is limited to investigate the effect of varying the thickness of the end-plate. In the study, the energy dissipation E_d is taken as the plastic dissipation in the region enclosing the joints, as defined in Figure 10. Frictional dissipation is neglected here because Abaqus does not support acquiring it from a specific region.
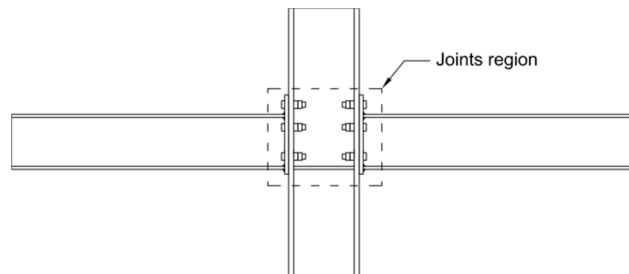

Figure 10 - Region considered for evaluating energy dissipation.

6.1 Results

Figure 11 shows curves with accumulated energy dissipation E_d versus displacement D of the column obtained from the simulations of an impact test at 12 m/s and a quasi-static test. The maximum value of the displacement D represents the ability of the joints to deform. This ductility measure is another important property of joints. Figure 11 clearly displays that the maximum displacement D obtained for the impact simulation is larger than for the quasi-static simulation. The reason for this significant difference is related to inertia effects, as elaborately discussed by Grimsmo et al. [9]. Figure 11 also shows that energies of approximately 14 and 8 kJ were dissipated in the impact and quasi-static simulations, respectively. The difference in energy dissipation is mainly related to the difference in displacement D at fracture for the two load cases. These energy dissipation values acquired from the simulations agree somewhat with the values determined from the experiments, where the dissipated energy was approximately 20 and 8.5 kJ in the impact and quasi-static tests, respectively [9]. Note that these experimental estimates include energy lost due to friction and plastic dissipation from the entire test specimen and set-up, which may explain the higher values compared to the simulations. This is particularly relevant for the impact tests, where some plastic deformation of the web of the column was observed in the vicinity of the point of impact. An interesting feature in Figure 11 is the sudden increase in the dissipation at a displacement D of approximately 5 mm, which occurred only for the impact simulation. This was caused by the inertia of the specimen inducing a deformation mode involving greater shearing action than in the quasi-static simulation. More specifically, the column displaced axially relative to the connected end-plates and beams such that the bolts experienced shear deformation and the bolt holes became plastically elongated. This shearing action also occurred in the tests, as discussed by Grimsmo et al. [9, 16].
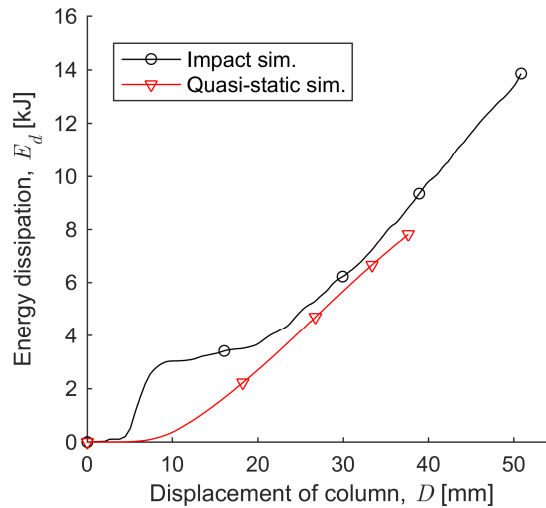
Figure 11 - Energy dissipation in simulations of impact and quasi-static tests.

With the script that generates the model, the user can readily explore favourable changes to the design of the joint configuration under impact load conditions. Here, it was chosen to investigate the effect of changing the end-plate thickness from the 12 mm used in the experiments to 9 and 15 mm. Such a considerable variation of the thickness was chosen because it induced a pronounced change in the response, and it does not necessarily represent a favourable design of the joint. The results are presented in Figure 12. Note that varying the plate thickness implies a corresponding change in the clamp length of the bolt and nut assemblies, which affects the tensile deformation capacity of the bolts. Figure 12a shows that both the energy dissipation E_d and the displacement D at failure with the 9 mm end-plate is approximately two times greater than with the two other end-plate thicknesses. Figure 12b depicts that the thinner end-plate experienced significant bending deformation, which allowed for increased displacement D, and thus more energy dissipation E_d, before failure.

a) Energy dissipation as a function of the displacement of the column

b) Deformed joint upon fracture with 15 mm (top) and 9 mm (bottom) end-plate
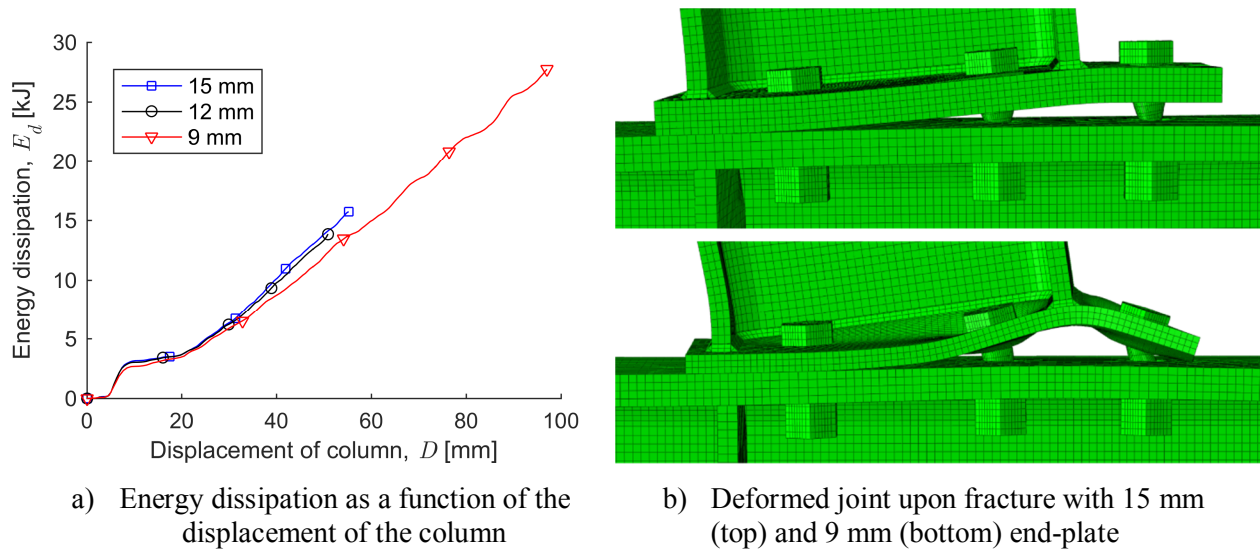
Figure 12 - Effect of varying the end-plate thickness in simulations of impact tests.

6.2 Discussion

With 9 mm thick end-plates, fracture occurred in the centre bolt (row) after significant yielding of the end-plates. This behaviour is reasonable because the calculation procedure following NS-EN 1993-1-8: *Design of joints* [17] (EC3) predicts that failure mode 2 (i.e., combined end-plate yielding and tensile bolt fracture) gives the lowest resistance for the centre bolt row when using 9 mm end-plates. For the simulation with 15 mm end-plates, failure was initiated by fracture of the right-most bolt (row) without considerable end-plate deformations. This behaviour is also reasonable because EC3 [17] calculations predict that failure mode 3 (i.e., tensile bolt fracture) gives the lowest resistance for the right-most bolt row when using 15 mm end-plates. Thus, the simulations with 9 and 15 mm end-plates can be considered within the validation domain of the numerical model based on the arguments above and that the deformation and failure modes in Figure 12b are similar to those of the validated model; see Figure 6a. However, recall that possible failure of the welds is not considered in these simulations. Coelho et al. [18] showed that failure by weld fracture may occur in connections that experience significant end-plate bending deformations.

Reducing the end-plate thickness from 12 to 9 mm increased the energy dissipation before failure by 100% because the deformation capacity of the end-plates was better utilized. However, this thickness reduction decreased the static bending moment resistance and initial rotational stiffness by 23% and 21%, respectively. These two properties are important for the static behaviour of the

joint. Increasing the thickness to 15 mm enhanced the energy dissipation by 14%, whereas the moment resistance and stiffness increased by 12% and 9%, respectively. Here, the energy dissipation was determined from the curves in Figure 12a, and the values of the static bending moment resistance and initial rotational stiffness were obtained from the calculation procedure following EC3 [17]. Based on these values, choosing the 15 mm end-plate may provide the greatest benefit for a given case because it has a positive effect on all three properties evaluated here, i.e. energy dissipation capacity, bending moment resistance, and initial rotational stiffness. In practice, the designer should assess the importance of each of these properties together with other aspects such as the tying resistance, financial cost, and ease of assembly.

As in the tests, the energy dissipated by the joint was higher in the impact simulation than in the quasi-static simulation. Grimsmo et al. [9] argued that there were several possible reasons for the increase in dissipation in the impact tests: the impact loading imposed a shear deformation of the bolts and plastic elongation of the bolt holes; enhanced stress levels due to higher strain rates; and a more symmetrical deformation mode, causing fracture to occur at a larger displacement D of the column. The findings from the simulations support these claims.

7   Effect of axial forces in the beams

The design code NS-EN 1991-1-7: *General actions – Accidental actions* [19] recommends that buildings of high consequence classes have adequate horizontal ties (e.g., beams) to ensure sufficient structural robustness. This means that the ties and their connections should be able to withstand a certain tensile load. Therefore, it is interesting to study how tensile axial forces in the beams affect the behaviour of the current joint configuration. Yang and Tan [3] measured a maximum axial force in the beams of about 400 kN in quasi-static tests with similar but larger test specimens subjected to column-loss load conditions and thus catenary action. Based on this reference, axial forces of approximately 150 and 300 kN were chosen for the numerical investigation here. These forces correspond to about 10% and 20% of the nominal axial yield resistance of the beams and 40% and 80% of the nominal tensile resistance of the end-plate connections according to the resistance formulas in EC3 [17]. A constant axial tension force was introduced by applying a constant negative surface pressure to the end-section of the beams in a separate step prior to the step where the impact occurred. Since any friction developed on the

supports would influence the effective axial force in the beams, the friction coefficient between the beam and support was set to zero in this investigation.

7.1   Results

The deformation and failure modes of the specimen were not appreciably affected by the presence of axial forces. In particular, the deformation of the end-plate region upon failure was similar to that observed in Figure 6a, and failure still occurred by tensile bolt fracture in the centre bolt row. As expected, however, the additional tensile force experienced by the bolts gave fracture at a reduced displacement D of the column as the axial force in the beams was increased. Fracture occurred at displacements of 50.9, 49.3, and 46.6 mm for axial forces of 0, 150, and 300 kN, respectively.

Figure 13a presents force-displacement curves obtained from the axial force study. By observing the first peak in the figure, it is clear that the axial forces did not affect the intial impact. However, the second impact occurred at a larger displacement D when the axial force was increased. This observation can be explained by Figure 13b, which presents curves of the velocity V of the column versus time. The figure reveals that increasing the axial force produced a slightly lower deceleration of the column during the non-contact period (approximately 1 to 4 ms). For the second hit, the trolley thus impacted the specimen at a later instant than for the case with no axial force. The reduced deceleration indicates that the moment resistance of the joints decreased due to the axial forces. This is reasonable because the moment resistance is partly governed by the tensile resistance of the bolts, and here, the bolts experience additional tensile forces introduced by the axial force. Thus, the contribution from the bolts to the moment resistance is reduced. Furthermore, the displacement D of the column is not sufficiently large for the axial force to activate any significant geometrical stiffness in the column and beam assembly.

a) Force versus displacement of column   b) Velocity of column versus time
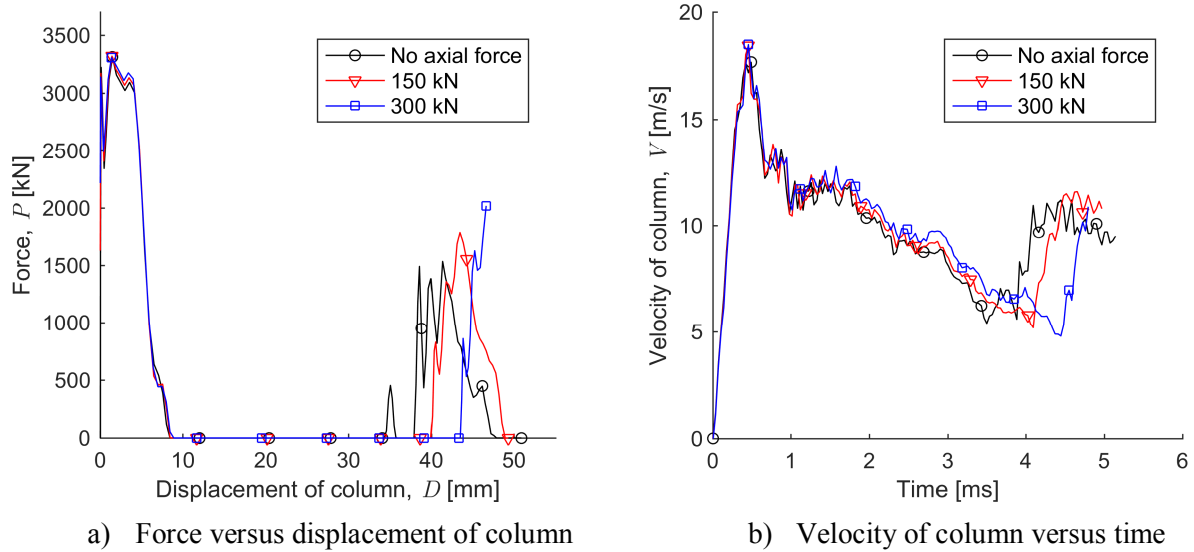
Figure 13 - Results from varying the axial force in the beams.

7.2   Discussion

Lima et al. [20] and Silva et al. [21] tested beam-to-column joints with end-plate connections subjected to combined bending and axial force. They observed that the moment resistance of the joints decreased with increasing tensile axial force, which supports the findings of the current investigation.

In reality, the axial forces in the beams of a framed structure depend on the deformation of the structural members and are therefore not constant. An axial force that varies with deformation might have affected the behaviour of the joints somewhat differently. Furthermore, large compressive axial forces in the beams may also arise under extreme situations. Although not investigated here, compressive axial forces in the beams tend to increase the moment resistance of joints with end-plate connections [20, 21].

8   Increased inertia of the beams

Inertia plays a significant role in the assessment of the response of a structure subjected to impact loading. For the joint configuration at hand, it is therefore relevant to consider the mass from structural members such as floor slabs attached to the beams. It is challenging to evaluate this issue in physical tests. Therefore, the FE model represents a useful tool for investigating the effects of inertia. Assuming that typical pre-cast concrete slabs are attached to the beams, a realistic estimate

of the mass distributed along the beams could be 1400 kg/m. This distributed mass was introduced in the numerical model by simply increasing the mass of the entire top layer of elements in the appropriate beam flanges. All other aspects of the model were retained.

8.1 Results

Figure 14 provides a cross-sectional view of the end-plate region as it deforms together with fringe plots of the Mises stress. Shear fracture of the bolts clearly occurred, in contrast to the previous simulations, where tensile fracture of the bolts took place. This is due to the additional forces required to accelerate the beams with the higher mass, which further caused the bolts to experience larger shear forces. Failure of the joints occurred at a displacement D of the column of approximately 18 mm. This represents a significant reduction of the ductility of the joint compared to the simulation without the additional mass, where the displacement at failure was 51 mm; see Section 5.1.

The effect of the increased inertia is also clearly observed in the force-displacement and velocity-time curves shown in Figure 15, where the results obtained with the validated model presented in Section 5.1 are included for comparison. In terms of the force-displacement curves in Figure 15a, the first impact was virtually unaffected by the additional inertia of the beams. However, the second impact occurred at a significantly smaller column displacement, and the force level was much higher compared to the second impact for the validated model. Considering the velocity-time curves in Figure 15b, the two models produced a similar response during the first 0.5 ms. At the end of this period, the end-plates and beams were activated. For the model with the larger inertia of the beams, the column was then more rapidly decelerated, leading to the second impact occurring at an earlier stage. The difference in the maximum force level of the second impact is explained by the difference in the relative velocity between the trolley and the column at the time of this impact. For the model with increased inertia of the beams, the velocity V of the column was 2.8 m/s for the second impact (at approx. 1 ms), whereas it was 4.9 m/s (at approx. 4 ms) for the validated model. As for the validated model (see Figure 7c), the velocity of the trolley during the non-contact period, and thus at the time of the second impact, was approximately 10 m/s in both cases.
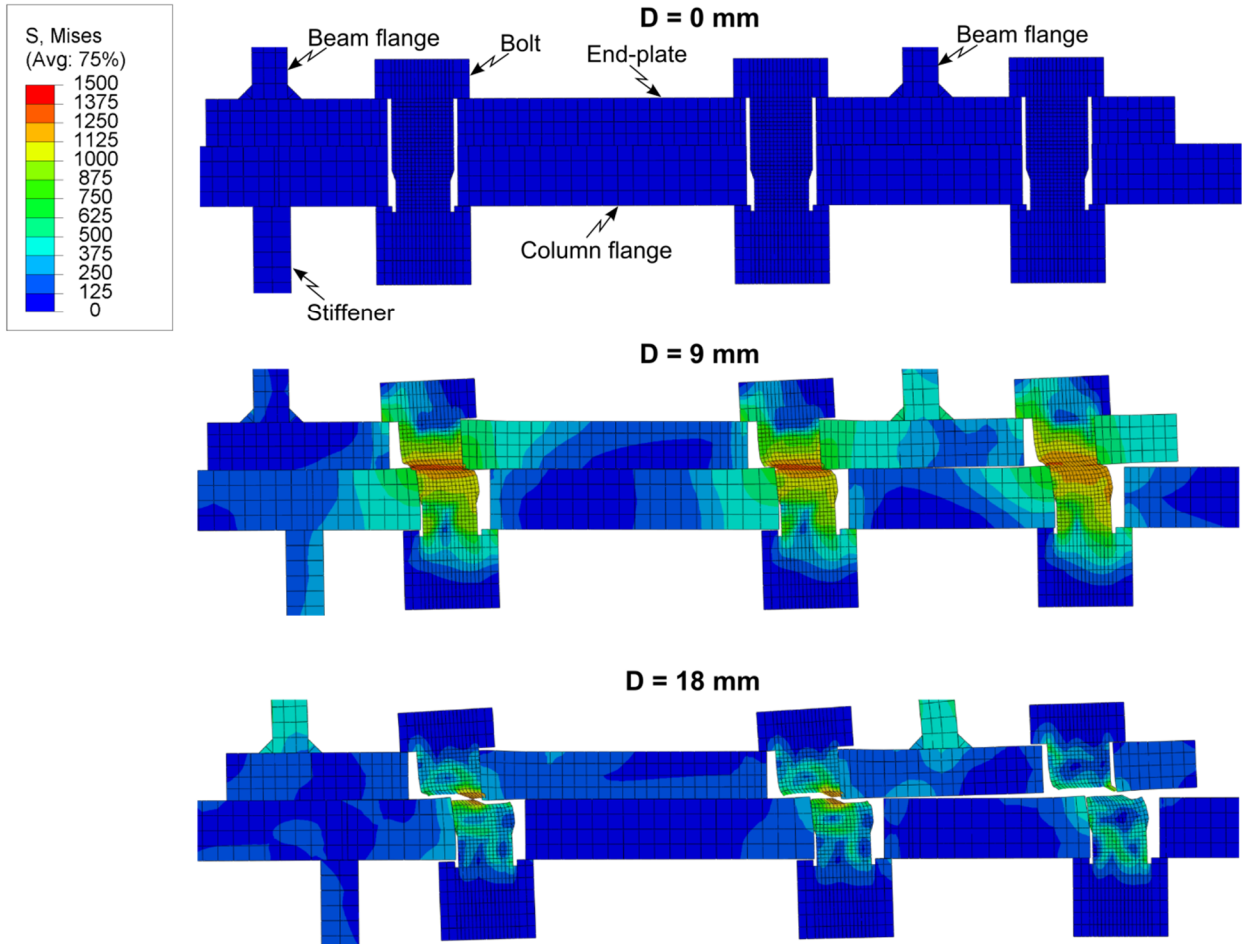
Figure 14 - Cross-sectional view of end-plate region at three stages of the displacement *D* of the column in a simulation where the mass of the beams has been increased.

a)   Force versus displacement of column   b)   Velocity of column versus time
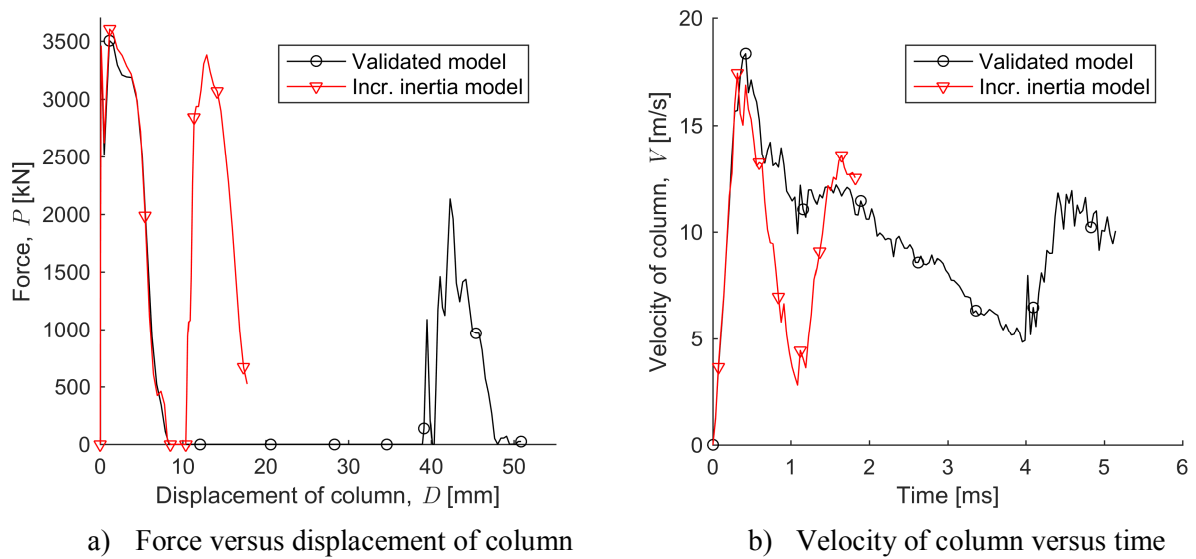
Figure 15 - Response obtained from numerical simulations with increased mass of the beams and with the validated model presented in Section 5.1.

8.2   Discussion

This investigation is qualitative in the sense that the purpose is only to provide an indication of the effects of considering the inertia of members such as floor slabs. To properly capture the shear fracture of the bolts, a significantly finer mesh is probably required because the thickness of the shear bands of high-strength steels subjected to high strain rates can be approximately 10 μm, as Kane et al. [22] observed in their perforation tests. Furthermore, attached floor slabs can affect the rotational stiffness, moment resistance, and rotational capacity of the joints, as demonstrated by Xiao et al. [23]. However, these effects were not considered here. Regardless, the performed simulations reveal that shear failure is a possible failure mode under impact load conditions. This change in failure mode resembles the phenomenon that can occur for structural members such as beams and floor slabs subjected to extreme impulsive loading. Specifically, the members can fail in direct shear in the vicinity of the supports before a flexural mode of response develops [24, 25].

Note that thermal softening was a prerequisite for obtaining shear failure in the current investigation. Although not shown here, increasing the length of the beams together with the distance to the supports does not affect the response because only approximately 250 mm of the beam length from the end-plates was activated prior to bolt failure. Thus, the inertia of the beams only in the vicinity of the joints is important here.

9   Summary and conclusions

FE simulations of impact tests on a double-sided, beam-to-column joint configuration have been performed. The numerical model was developed with three-dimensional elements and an elastic-thermoviscoplastic material model incorporating work-hardening, strain-rate sensitivity, thermal softening, and failure. The simulations captured the deformation and failure mode observed in the tests. Furthermore, the global response in terms of force-displacement and velocity-time curves agreed with the tests. These comparisons of local and global behaviour served as a validation of the numerical model. The validated model allowed investigating issues that are challenging and costly to investigate in physical tests. It was chosen to study the effects of changing the thickness of the end-plate, introducing tensile forces in the beams and increasing the mass of the beams. Essential observations and conclusions from these studies are:

1) Reducing the end-plate thickness allowed greater bending deformation of the end-plate before bolt fracture. Consequently, the energy dissipated by the joint was significantly increased. Thus, using thinner end-plates seems beneficial for impact load conditions.

2) Imposing significant tensile axial forces in the beams barely affected the response of the joint configuration. The displacement to failure, which represents the ductility of the joint, was somewhat reduced with increasing axial force. Nevertheless, the general behaviour, such as the deformation and failure mode, was practically the same as without axial forces. Thus, for the joint configuration at hand, it is not imperative to consider axial forces in the beams.

3) Taking the additional mass from structural elements such as possible floor slabs into account could affect the failure mode. A simulation with increased inertia of the beams was conducted. In this simulation, the failure mode changed from tensile to shear fracture of the bolts, which led to reduced global deformation prior to failure. These observations highlight how inertia effects may significantly alter the dynamic response compared to the quasi-static response.

In conclusion, FE simulations with a validated numerical model can be useful for evaluating the behaviour of joints under severe impulsive load conditions.

Acknowledgements

Appendix

This appendix provides additional information that enable the reader to build the FE models presented in this paper. Figure A.1 provides the details of the test specimen, and Figure A.2 shows the dimensions of the impact plate.

a) Elevation view.

b) Cross-sectional (A-A) view of the beam and end-plate.

Figure A.1 - Dimensions of the test specimen. Adapted from Figure 1 in [9].

Figure A.2 - Dimensions of the impact plate.

The bolt and nut assembly was modelled as one part in this paper. The dimensions of the part are given in the section drawing in Figure A.3. As observed from the figure, an additional length of

the shank of 1.5 mm was included to account for the countersink of the nut. Two nuts were used in the tests to avoid thread stripping, which explains the height of 20 mm of the portion representing the nut.
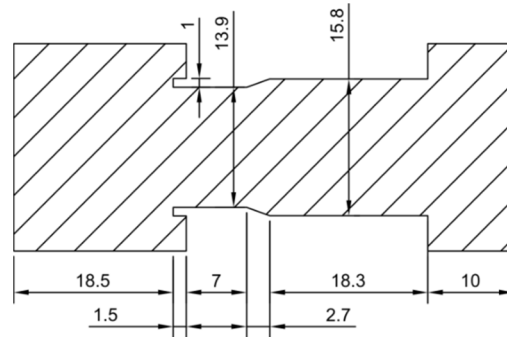

Figure A.3 - Cross-sectional view of the bolt and nut assembly model.

References

[1]   Department of Defence (DOD), Structures to resist the effects of accidental explosions: Unified Facilities Criteria (UFC 3-340-02), US Department of Defence, Alexandria, VA, 2008.

[2]   T. Sabuwala, D. Linzell, T. Krauthammer, Finite element analysis of steel beam to column connections subjected to blast loads, Int J Impact Eng, 31 (2005) 861-876.

[3]   B. Yang, K.H. Tan, Experimental tests of different types of bolted steel beam-column joints under a central-column-removal scenario, Eng Struct, 54 (2013) 112-130.

[4]   C. Liu, K.H. Tan, T.C. Fung, Dynamic behaviour of web cleat connections subjected to sudden column removal scenario, J Constr Steel Res, 86 (2013) 92-106.

[5]   C. Liu, K.H. Tan, T.C. Fung, Investigations of nonlinear dynamic performance of top-and-seat with web angle connections subjected to sudden column removal, Eng Struct, 99 (2015) 449-461.

[6]   C. Liu, K.H. Tan, T.C. Fung, Dynamic performance of flush end-plate beam-column connections and design applications in progressive collapse, J Struct Eng-ASCE, (2015).

[7]   A. Tyas, J.A. Warren, E.P. Stoddart, J.B. Davison, S.J. Tait, Y. Huang, A Methodology for Combined Rotation-Extension Testing of Simple Steel Beam to Column Joints at High Rates of Loading, Exp Mech, 52 (2012) 1097-1109.

[8]   R. Rahbari, A. Tyas, J. Buick Davison, E.P. Stoddart, Web shear failure of angle-cleat connections loaded at high rates, J Constr Steel Res, 103 (2014) 37-48.

[9]   E.L. Grimsmo, A.H. Clausen, M. Langseth, A. Aalberg, An experimental study of static and dynamic behaviour of bolted end-plate joints of steel, Int J Impact Eng, 85 (2015) 132-145.

[10]   V. Vilamosa, A.H. Clausen, E. Fagerholt, O.S. Hopperstad, T. Børvik, Local measurement of stress-strain behaviour of ductile materials at elevated temperatures in a split-Hopkinson tension bar system, Strain, 50 (2014) 223-235.

[11] M.G. Cockcroft, D.J. Latham, Ductility and the workability of metals, J I Met, 96 (1968) 33-39.

[12] G. Gruben, O.S. Hopperstad, T. Borvik, Evaluation of uncoupled ductile fracture criteria for the dual-phase steel Docol 600DL, Int J Mech Sci, 62 (2012) 133-146.

[13] T. Børvik, S. Dey, A.H. Clausen, Perforation resistance of five different high-strength steel plates subjected to small-arms projectiles, Int J Impact Eng, 36 (2009) 948-964.

[14] D. Systémes, Abaqus 6.14 documentation, Simulia Systems, Providence, RI, 2014.

[15] European Committee for Standardization (CEN), NS-EN 1090-2:2008+A1:2011, execution of steel structures and aluminium structures - part 2: technical requirements for steel structures, Norwegian Standard, 2008.

[16] E.L. Grimsmo, A.H. Clausen, A. Aalberg, M. Langseth, Beam-to-column joints subjected to impact loading, in: Nordic Steel Construction Conference, Tampere, Finland, 2015.

[17] European Committee for Standardization (CEN), NS-EN 1993-1-8:2005, Eurocode 3: design of steel structures - part 1-8: design of joints, Norwegian Standard, 2009.

[18] A.M. Girão Coelho, F.S.K. Bijlaard, L. Simões da Silva, Experimental assessment of the ductility of extended end plate connections, Eng Struct, 26 (2004) 1185-1206.

[19] European Committee for Standardization (CEN), NS-EN 1991-1-7, Action on structures - part 1-7: general actions - accidental actions, Norwegian Standard, 2006.

[20] L. Lima, L. Simões da Silva, P. Vellasco, S. Andrade, Experimental evaluation of extended endplate beam-to-column joints subjected to bending and axial force, Eng Struct, 26 (2004) 1333-1347.

[21] L. Simões Da Silva, L. Lima, P. Vellasco, S. Andrade, Behaviour of flush end-plate beam-to-column joints under bending and axial force, Steel Compo Struct, 4 (2004) 77-94.

[22] A. Kane, T. Børvik, O.S. Hopperstad, M. Langseth, Finite element analysis of plugging failure in steel plates struck by blunt projectiles, J Appl Mech-T ASME, 76 (2009) 1-11.

[23] Y. Xiao, B.S. Choo, D.A. Nethercot, Composite connections in steel and concrete. I. Experimental behaviour of composite beam—column connections, J Constr Steel Res, 31 (1994) 3-30.

[24] S.B. Menkes, H.J. Opat, Broken beams - Tearing and shear failures in explosively loaded clamped beams, Exp Mech, 13 (1973) 480-486.

[25] T. Krauthammer, Modern Protective Structures, CRC Press, Taylor & Francis Group, Boca Raton, FL, 2008.